Proceedings of IPACK2007
ASME InterPACK '07
July 8-12, 2007, Vancouver, British Columbia, CANADA

IPACK2007-33878

OPTIMIZATION OF SI/SIGE MICROREFRIGERATORS FOR HYBRID SOLID-STATE/LIQUID COOLING

Y. Ezzahri, R. Singh, J. Christofferson, Z. Bian,
and A. Shakouri
Department of Electrical Engineering, University of
California Santa Cruz, California
95064 USA

ABSTRACT

Monolithic Solid-state microrefrigerators have attracted a lot of attention during the last ten years since they have the potential to solve some of the problems related to localized heat generation and temperature stabilization in optoelectronic, microelectronics or even biological microchip applications. Combination of the solid-state cooling with other conventional techniques like liquid cooling, offers an additional degree of freedom to control both the overall temperature of the chip and to remove hot spots. We present a new approach based on Thermal Quadrupoles Method to model the behavior of a single stage Si/SiGe microrefrigerator in the DC operating regime. The sensitivity and precision of this method come from its analytical expressions, which are based on the solution of Fourier's heat diffusion equation in the Laplace domain. The microrefrigerator top surface temperature is calculated by taking into account all possible mechanisms of heat generation and conduction within the entire device. The 3D heat and current spreading in the substrate is taken into account. The parasitic heat leakage to the cold junction due to heat generation and heat conduction within the metal lead is also considered. The theoretical results are then compared with experimental ones for several microrefrigerator sizes. A good agreement is found between them. Based on the simulations, the structure of the microrefrigerator is optimized for lowering the overall chip temperature and removing high power density hot spots in several applications in conjunction with liquid cooling techniques.

INTRODUCTION

Thermoelectric coolers are used for temperature stabilization and control of microelectronic and optoelectronic components. Due to an increasing demand for localized cooling and temperature control in the last ten years, nanostructured cooling devices have attracted a lot attention for their potential use in hot spot removal in microelectronic and optoelectronic devices. The nanostructured materials have manifested very interesting thermoelectric properties, enabling them to have a figure-of-merit *ZT*, exceeding *1* at room temperature. The *ZT* is defined by $ZT = \frac{\sigma S^2}{\beta} T$, where σ, S, and β are respectively the electrical conductivity, Seebeck coefficient and thermal conductivity of the thermoelectric material. SiGe is a well known bulk thermoelectric material for high temperature power generation applications. Recently, Si/SiGe superlattice structures have been investigated for room temperature applications [1]. Si-based microrefrigerators are attractive for their potential monolithic integration with Si microelectronics. Another advantage of these devices is their ability to be combined with other conventional liquid cooling techniques [2], which can offer an additional degree of freedom to both remove background heating and hot spots.

In this paper, we use Thermal Quadrupoles Method (TQM) [3] to optimize the microrefrigerator maximum cooling and maximum cooling power density as a function of several geometrical parameters and material properties; we will focus especially on the properties of the active Si/SiGe layer and the substrate. In this single element devices, Joule heating and heat conduction in the contact metallization to the cold junction could reduce the device performance significantly and the geometry and thickness of this metallization should be optimized. The TQM is a general analytical model that can be used to calculate electrical and thermal responses in the AC regime, thus making it possible to distinguish, in some cases, the Peltier effect from the Joule effect. In the case of a pure sine wave electrical excitation, the Peltier effect appears at the same frequency as the operating current, whereas the Joule effect appears at the double frequency. The precision of TQM allows its application in the detailed characterization of thermoelectric

material properties [4]. This method has been used to model the behavior of a conventional thermoelectric couple (Bi_2Te_3) [5], and recently the behavior of Si/SiGe microrefrigerator [6]. The model presented here uses the limit of the TQM at long times (i.e. steady-state behavior). Thermophysical properties of the microrefrigerator are assumed to be temperature independent. In this model, the microrefrigerator top surface temperature variation is calculated by taking into account all possible mechanisms of heat generation and conduction within the entire device. 3D Heat and current spreading in the substrate is taken into account. Heat generation in the metal leads connected to the cold junction and also heat conduction through these leads are also calculated via TQM. All these features make this model more consistent, more complete and closer to real devices, than the previous work of D. Vashaee et al [7, 8], and Y. Ezzahri et al [6].

NOMENCLATURE

β_i: thermal conductivity of medium i.
σ_i: electrical conductivity of medium i.
Σ_i: cross sectional area of medium i.
θ_{in}: temperature at the input of the medium.
θ_{out}: temperature at the output of the medium.
ϕ_{in}: heat flux at the input of the medium.
ϕ_{out}: heat flux at the output of the medium.
h_{eff}: effective heat transfer coefficient describing heat conduction within the substrate.
I_e: amplitude of the excitation current.
$l_x=l_b=l_m$: length of the metal lead.
J: Joule heat source.
P: Peltier heat source.
r: radius of the contact disc at the microrefrigerator/ substrate interface.
R^{the}: thermal resistance.
R^{ele}: electrical resitance.
S_i: absolute Seebeck coefficient of medium i.
T_0: room temperature.
$w_x=w_b=w_m$: width of the metal lead.
ZT: figure of merit.

SAMPLE DISCRIPTION

Figure 1 (a) shows a Scanning Electronic Microscope (SEM) picture of a set of Si/SiGe microrefrigerators with five different sizes. Figure 1 (b) illustrates the schematic cross-sectional view of a Si/SiGe microrefrigerator that we consider in our simulation. The detailed composition of the device can be found in references [9, 10].

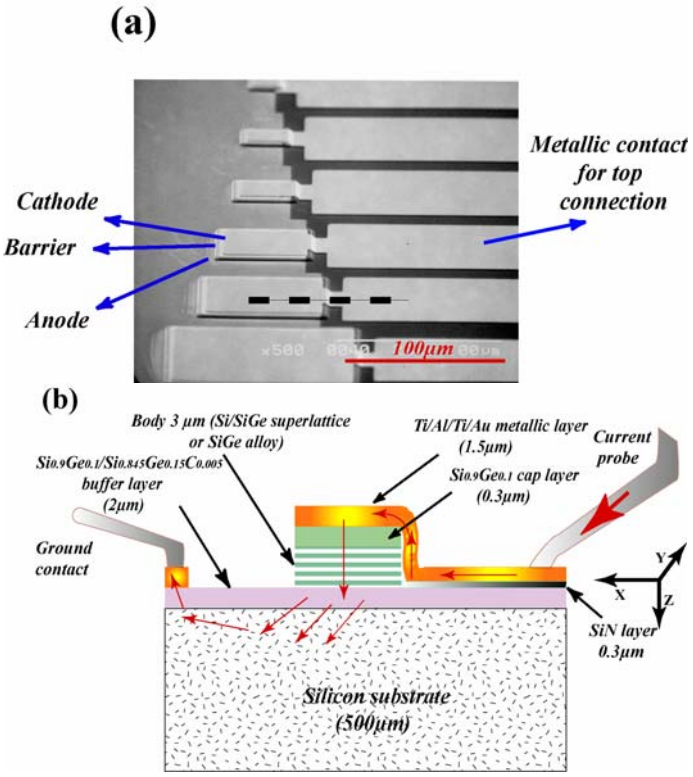

Figure 1: (a) SEM picture of a set of microrefrigerators with five different sizes, and (b) Schematic diagram of the microrefrigerator cross sectional view. Arrows indicate the direction of the electron flux. X is the direction of the metal lead at the top side, Z is the cross plan direction, and Y is the complementary direction.

THERMOELECTRIC AND THERMIONIC COOLING

In a Si/SiGe microrefrigerator, the Peltier cooling occurs at the top metal layer/SiGe active layer junction and also at the buffer layer/substrate junction when the device is fed by a current. The density of heat exchanged with the surrounding medium is characterized by the effective Seebeck coefficient difference at these junctions, and it is proportional to both current intensity and junction temperature [1]. Because of the difference in the Seebeck coefficient values at various interfaces Peltier cooling or heating is created depending on the direction of the electrical current [1].

In the case where the active layer is a superlattice structure, in addition to thermoelectric cooling, there is a thermionic cooling as it was shown by A. Shakouri et al [11-12] and G. D. Mahan et al [13], which is an evaporative selective hot electrons filtering effect. Assuming small current densities, we can define an effective Seebeck coefficient for the solid-state thermionic cooling analogous to linear thermoelectric effects. Heating or cooling density at interfaces can then be considered as a linear function of the current [11-14]. In our model, we assume that the effective Seebeck coefficient takes into account both thermoelectric and thermionic phenomena.

THEORETICAL MODEL AND SIMULATION

Our theoretical model is based on the limit of the TQM at long times. Layer thicknesses are several orders of magnitude larger than the mean free path of both electrons and phonons [15]. We can hence assume a diffusive transport regime, and Fourier Diffusion Heat Equation (FDHE) can then be used. When the active layer is a superlattice, because individual layers within it are very thin, on the order of nanometers, the superlattice is considered as an effective medium.

HEAT TRANSPORT IN THE CROSS-PLAN DIRECTION OF THE MICROREFRIGERATOR

Let us assume a one-dimensional heat transfer in Laplace domain for a passive, linear, homogeneous and isotropic medium. The solution of the FDHE under adiabatic conditions gives a linear relationship between temperature-flux vectors at both ends of the medium in the form:

$$\begin{pmatrix} \theta_{in} \\ \phi_{in} \end{pmatrix} = \begin{pmatrix} 1 & R_i^{the} \\ 0 & 1 \end{pmatrix} \begin{pmatrix} \theta_{out} \\ \phi_{out} \end{pmatrix} \quad (1)$$

where: $R_i^{the} = \dfrac{t_i}{\beta_i \Sigma}$, β_i, t_i, and Σ_i are respectively thermal conductivity, thickness and the cross sectional area of the isothermal surface in the medium. $\begin{pmatrix} \theta_{in} \\ \phi_{in} \end{pmatrix}$ and $\begin{pmatrix} \theta_{out} \\ \phi_{out} \end{pmatrix}$ are the Laplace transforms of temperature and heat flux vectors at the input and the output of the medium, respectively.

The thickness of the active SiGe layer is very small compared to that of the substrate; moreover, all Peltier sources are uniform at all junction plans. We thus consider the heat transfer across the microrefrigerator to be one-dimensional in the cross-plan direction of the device. We neglect heat transfer at the side surface area around the mesa due to convection and radiation. We assume adiabatic conditions at these surfaces. This can be justified due to the small dimensions of the microrefrigerator and the marginal cooling temperature reduction. Our structure is formed of four essential layers; the transfer matrix of each layer can be written in the form:

$$\begin{pmatrix} \theta_{in} \\ \phi_{in} \end{pmatrix} = \begin{pmatrix} 1 & R_i^{the} \\ 0 & 1 \end{pmatrix} \begin{pmatrix} \theta_{out} \\ \phi_{out} \end{pmatrix} - \begin{pmatrix} \dfrac{R_i^{the}}{2} \\ 1 \end{pmatrix} \mathrm{J_i} \quad (2)$$

The term J_i indicates the internal Joule heating source inside each layer, and is given by:

$$J_i = R_i^{ele} I_e^2 \quad (3)$$

R_i^{ele} and I_e are the electrical resistance of each layer, and the amplitude of the excitation current respectively. The subscript *i=m, c, s, b* stands for the metallic layer, the cap layer, the active SiGe layer and the buffer layer, respectively.

HEAT TRANSPORT WHITIN THE SUBSTRATE

Regarding the local character of the microrefrigerator, the silicon substrate underneath it is considered thermally thick and its effect will be contained in what is called the *Resistance of constriction or spreading*. Constriction and spreading resistances exist whenever heat flows from one region to another of different cross sectional area. The term constriction is used to describe the situation where heat flows out from a large cross sectional region into a narrower one, and the term spreading is used to describe the opposite case where heat flows out of a narrow region into a larger cross sectional area.

Approximating both of the microrefrigerator and the substrate with a cylindrical geometry, the thermal constriction/spreading resistance is given by [3]:

$$R_{Sub}^{the,1} = \frac{8}{3\pi^2 \beta_s r} \quad (4)$$

where r is the radius of the contact disc between the two mediums, and β_s is the thermal conductivity of the substrate.

In fact, the expression of this constriction/spreading resistance depends on the form of temperature and heat flux distributions in the *[0, r]* interval. Equation (4) is valid in the case of uniform heat flux distribution in this interval which should match better the physics. One should note that the difference in the expressions of the constriction/spreading resistances for the case of uniform heat flux distribution and the case of uniform temperature distribution in the *[0, r]* interval is only *8%* [3]. In addition to the thermal spreading inside the substrate, there is an electrical current spreading. Joule heating is mainly localized at the buffer-layer/substrate interface [16]. This electrical spreading is characterized by a spreading of the electrical current density lines in the substrate. The electrical constriction/spreading resistance is calculated in analogy with the thermal resistance, and is given by the equation:

$$R_{Sub}^{ele} = \frac{8}{3\pi^2 \sigma_s r} \quad (5)$$

where r is the radius of the contact disc between the microrefrigerator and the substrate, and σ_s is the electrical conductivity of the substrate.

HEAT TRANSPORT WHITIN THE TOP SIDE CONTACT OF THE MICROREFRIGERATOR

The top side metal lead is provided to carry the current to the cold junction, but it turns out that it is responsible for some part of Joule heating, which limits the maximum cooling. The temperature change within this metal lead is dominant in the longitudinal direction (X direction) and, therefore, the metal lead can be viewed as a thermal fin. To describe heat transfer within this metal lead, P. Wang et al [17] have solved directly the heat diffusion equation in the longitudinal direction with two appropriate boundary conditions, which are: (i) a constant temperature at the interface metal lead/ microrefrigerator top surface, and (ii) a zero heat flux at the other end of the metal lead. In our analysis, we still use TQM in the longitudinal direction of the metal lead by assuming the same boundary conditions as P. Wang et al [17]. As for the microrefrigerator, the top metal lead surface is considered adiabatic, but heat conduction from the bottom surface of the metal lead through the SiN_x layer and the buffer layer into the silicon substrate

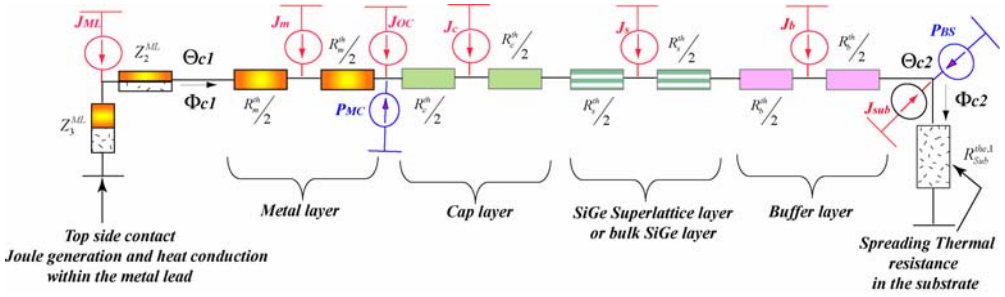

Figure 2: Thermal quadrupole network associated with the heat transfer within the whole SiGe microrefrigerator in a steady state regime

(see figure 1 (b)), is described by an effective heat transfer coefficient given by:

$$h_{eff} = \frac{1}{\left(R_{SiN_x} + R_{Buffer} + R_{Sub}^{the,2}\right) l_m w_m} \quad (6)$$

where R_{SiNx}, R_{Buffer} and $R_{Sub}^{the,2}$ are the thermal resistances of the SiN_x layer, the buffer layer and the substrate, respectively.

Heat conduction inside the SiN_x layer and the buffer layer is assumed to be one dimensional and perpendicular to the bottom surface of the metal lead. The corresponding thermal resistances are thus given by:

$$\begin{cases} R_{SiN_x} = \dfrac{t_x}{\beta_x l_x w_x} \\ R_{Buffer} = \dfrac{t_b}{\beta_b l_b w_b} \end{cases} \quad (7)$$

where t_x, t_b, β_x, β_b, are the thicknesses and the thermal conductivities of the SiN_x layer and the buffer layer, respectively. $l_x=l_b=l_m$ and $w_x = w_b = w_m = \sqrt{\Sigma}$ are the length and the width of the metal lead. Σ is the cross sectional area of the microrefrigerator.

As the length of the metal lead is larger than its width, the heat conduction downwards in the silicon substrate is assumed to take the form of two dimensional spreading (in Y-Z plane), and the average value of the spreading thermal resistance can be calculated as [17, 18]:

$$R_{Sub}^{the,2} = \frac{1}{2\beta_{Sub} l_m}\left[\delta + \frac{2}{\pi^3 \varepsilon^2}\sum_{n=1}^{\infty}\frac{\sin^2(n\pi\varepsilon)}{n^3}\tanh(n\pi\delta)\right] \quad (8)$$

where $\delta = {2t_{Sub}}/{w_{Sub}}$, and $\varepsilon = {w_m}/{w_{Sub}}$. t_{Sub}, W_{Sub}, and β_{Sub} are the thickness, the width and the thermal conductivity of the substrate, respectively. One can note here that the substrate underneath the metal lead is considered as a finite medium at the opposite of the microrefrigerator device. This is because of the relatively larger size of the side metal lead.

Application of TQM to the heat transfer along the metal lead, in combination with the second boundary condition (zero heat flux at the beginning of the metal lead) allows us to get the relation between the heat flux at the interface metal lead/ microrefrigerator and the temperature variation at the top surface of the later. In fact, it is easy to see that $\phi_{ML}^{in} = 0$ leads to:

$$\phi_{ML}^{out} = \phi_{C1} = R_{ML}^{ele}\sqrt{\frac{\beta_m t_m}{l_m^2 h_{eff}}}\,th\left(\sqrt{\frac{h_{eff}}{\beta_m t_m}}lm\right) I_e^2 - \sqrt{\beta_m t_m w_m^2 h_{eff}}\,th\left(\sqrt{\frac{h_{eff}}{\beta_m t_m}}lm\right)\theta_{C1} \quad (9)$$

where $R_{ML}^{ele} = \dfrac{lm}{\sigma_m w_m t_m}$, t_m and σ_m are the thickness and the electrical conductivity of the metal lead, respectively. More detail on how we obtain equation (9) by application of TQM, will be presented in a future work [19]. θ_{C1} represents the temperature variation at the top surface of the microrefrigerator. The first term of equation (9) describes Joule heating generation within the metal lead whereas the second term describes heat conduction due to the temperature gradient within it. Both of those effects will reduce the effective cooling rate of the microrefrigerator and thus degrade the cooling performance. We also demonstrated that the ohmic contact resistance R_C^{Ohm} between the cap layer and the metallic layer is another important limiting factor on the performance of the microrefrigerator.

THERMAL QUADRUPOLE REPRESENTATION

Figure 2 above, illustrates the quadrupole system associated with the whole microrefrigerator device. The application of Kirchhoff laws to this system, allows us to get a matrix relation, which represents the heat transfer in the whole structure between $\begin{pmatrix}\theta_{C1}\\ \phi_{C1}\end{pmatrix}$ and $\begin{pmatrix}\theta_{C2}\\ \phi_{C2}\end{pmatrix}$, the temperature-heat flux vectors at the top metallic layer and the interface buffer layer/substrate, respectively:

$$\begin{pmatrix}\theta_{C1}\\ \phi_{C1}\end{pmatrix}=\begin{pmatrix}1 & R_m^{the}+R_c^{the}+R_s^{the}+R_b^{the}\\ 0 & 1\end{pmatrix}\begin{pmatrix}\theta_{C2}\\ \phi_{C2}-P_{BS}-J_{Sub}\end{pmatrix}$$
$$-\begin{pmatrix}1 & R_m^{the}+R_c^{the}+R_s^{the}\\ 0 & 1\end{pmatrix}\begin{pmatrix}\frac{R_b^{the}}{2}J_b\\ J_b\end{pmatrix}-\begin{pmatrix}1 & R_m^{the}+R_c^{the}\\ 0 & 1\end{pmatrix}\begin{pmatrix}\frac{R_s^{the}}{2}J_s\\ J_s\end{pmatrix}$$
$$-\begin{pmatrix}1 & R_m^{the}\\ 0 & 1\end{pmatrix}\begin{pmatrix}\frac{R_c^{the}}{2}J_c\\ J_c+P_{MC}+J_{MC}\end{pmatrix}-\begin{pmatrix}\frac{R_m^{the}}{2}J_m\\ J_m\end{pmatrix} \quad (10)$$

where:

$$\begin{cases}P_{MC}=(S_M-S_s)I_eT_0,\ P_{BS}=(S_s-S_{Sub})I_eT_0\\ J_{Sub}=R_{Sub}^{ele}I_e^2, J_C^{Ohm}=R_C^{Ohm}I_e^2\\ \phi_{C2}=\dfrac{\theta_{C2}}{R_{Sub}^{the,1}}\end{cases} \quad (11)$$

S_M, S_s, and S_{Sub} are the absolute Seebeck coefficients of the metal layer, active SiGe layer, and substrate, respectively. The effective active layer Seebeck coefficients include both thermoelectric and thermionic contributions in the case where the active layer is a Si/SiGe superlattice, as we have mentioned above. T_0 is the average temperature of the junction that we take to be equal to the room temperature *300K* [6].

Combination of equations 9, 10, and 11 allows us to get the expression of the microrefrigerator top surface temperature variation θ_{C1} as a function of the excitation current amplitude I_e, as well as all physical and geometrical parameters of the whole device. The final point we shall discuss in this section is related to the cooling power density. This quantity is defined as the heat load mass added to the microrefrigerator top surface for which the temperature at this surface becomes zero.

RESULTS AND DISCUSSION

Before we present the result of the optimization, we start our discussion by ensuring the consistency of our model. For this we have used it to fit some of the experimental data. Figure 3 shows the results of this operation for two microrefrigerators with different device sizes, those microrefrigerators differ only by the nature of the active SiGe layer. In figure 3 (a) the active layer is an alloy, whereas in figure 3 (b), the active layer is a Si/SiGe superlattice. The thickness of the active layer is the same for both devices and equals *3 μm*. The cooling of the devices was measured using standard type E micro-thermocouple with a tip size of *50 μm* [20].

As we can see in Figure 4 above, both microrefrigerators with bulk SiGe and Si/SiGe superlattice produce almost the same cooling for each device size. Although separate 3ω measurements [21] show that bulk SiGe alloy has a thermal conductivity which is about *30%* lower than that of Si/SiGe superlattice, the later compensate this difference in the power factor as we can see in table 1 below. This table recapitulates material parameters of bulk SiGe alloy and Si/SiGe superlattice measured and estimated at room temperature for a *60×60μm²* device size. This is because of this compensation effect why the global cooling of the microrefrigerators is the same for the same device size [22]. The power factor σS^2 in the case of Si/SiGe superlattice is almost *24%* higher than the case with bulk SiGe alloy.

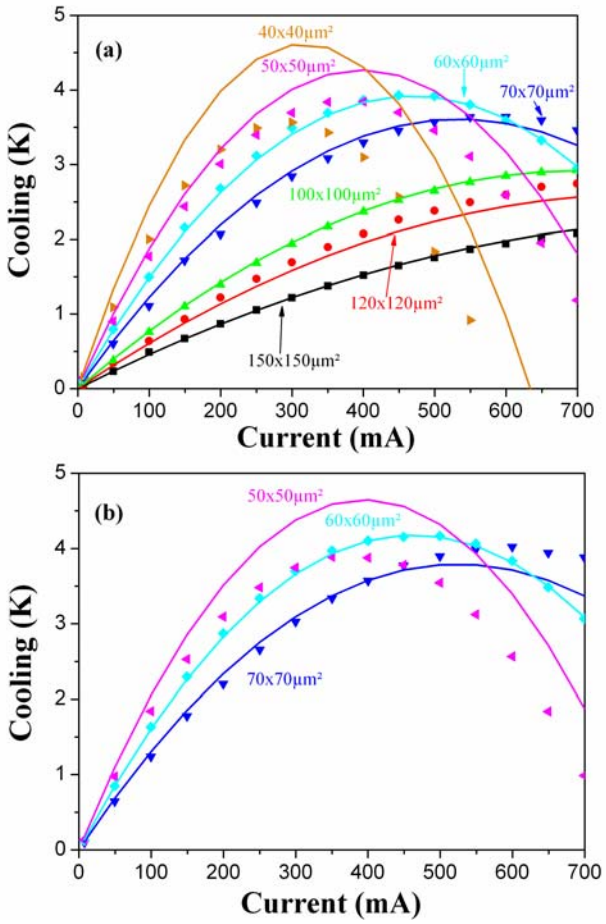

Figure 3: Measured cooling on thin film bulk SiGe microrefrigerator (a) and Si/SiGe superlattice microrefrigerator (b) for different device sizes, and their corresponding fit based on Thermal Quadrupoles Method**.**

Indeed, the physics behind the cooling effect is different for the two microrefrigerators; for the first one with SiGe alloy, the cooling is purely thermoelectric, whereas for the second one with Si/SiGe superlattice, in addition to thermoelectric cooling, there is a thermionic cooling, which consists on a selective evaporative emission of hot electrons from the cathode (cap layer) through the barrier (superlattice layer) to the anode (buffer layer).

The model fits very well big device sizes, but fails to fit small sizes (less than *50x50μm²*). In fact, for small device sizes, because of the thermal mass of the micro-thermocouple, cooling is underestimated.

Table 1: Material parameters for bulk SiGe alloy and Si/SiGe superlattice. Maximum cooling temperature of microrefrigerator devices based on some of the material is also given. Typical microrefrigerator device size is $60\times60\ \mu m^2$ and thin film thickness is $\sim3\ \mu m$. (∥) refers to in-plane material properties and (⊥) refers to cross-plane material properties. The estimated cross-plane power factors and *ZTs* for superlattices are based on the measured maximum cooling of microrefrigerators and the comparison with identical thin film devices based on alloy material. * refers to values used to get the best fit for all microrefrigerator sizes. ^ refers to the calculated power factors and *ZTs* based on the best fit parameters.

Material	S (μV/K)	σ (Ω/cm^2)	β (W/m/K)	$S^2\sigma$ (10^{-3} $W/K^2/m$)	ZT
$Si_{0.8}Ge_{0.2}$ alloys ΔT_{max}=4.0K	210 210*	367 375*	5.9 6*	1.6* 1.7^	0.08 0.083^
$Si/Si_{0.75}Ge_{0.25}$ (3nm/12nm) ΔT_{max}=4.2K	200-220 (⊥) 235* 180 (∥)	384 (∥) 384*	6.8-8.7 (⊥) 8*	2.2 (⊥ estimated) 1.2 (∥) 2.1^	0.085 (⊥ estimated) 0.080^

Now after model validation, let us see how we can use the model to optimize the cooling performance of the microrefrigerator. To study how the maximum cooling and maximum cooling power density are affected by the geometrical and physical properties of the microrefrigerator and to find methods of optimizing its performance, a series of simulation are performed and they are presented below. We start by discussing the dependence of the maximum cooling and the maximum cooling power density on both the cross sectional area of the microrefrigerator and the thickness of the active layer. Figure 4 shows the variation of the maximum cooling (a) and the maximum cooling power density (b) as a function of the cross sectional area of the microrefrigerator and the thickness of the active SiGe layer. As we can see in figure 4 (a), the maximum cooling is increasing monotonically with respect to the variables, i.e. the optimum device size increases by increasing the active layer thickness and vice versa. On the other hand, the maximum cooling power density (see figure 4 (b)) is decreasing monotonically with respect to the variables as it is expected.

The maximum thickness of the Si/SiGe superlattice depends on the growth time and for MBE growth we can take the value of $10\ \mu m$. We take this thickness as fixed, and we look to the behavior of the maximum cooling and the maximum cooling power density as a function of the microrefrigerator cross sectional area for different values of the Ohmic contact resistances at the interface metal layer/cap layer. It turns out that this parameter is the most important parasitic factor limiting the cooling performance of the microrefrigerator [20].

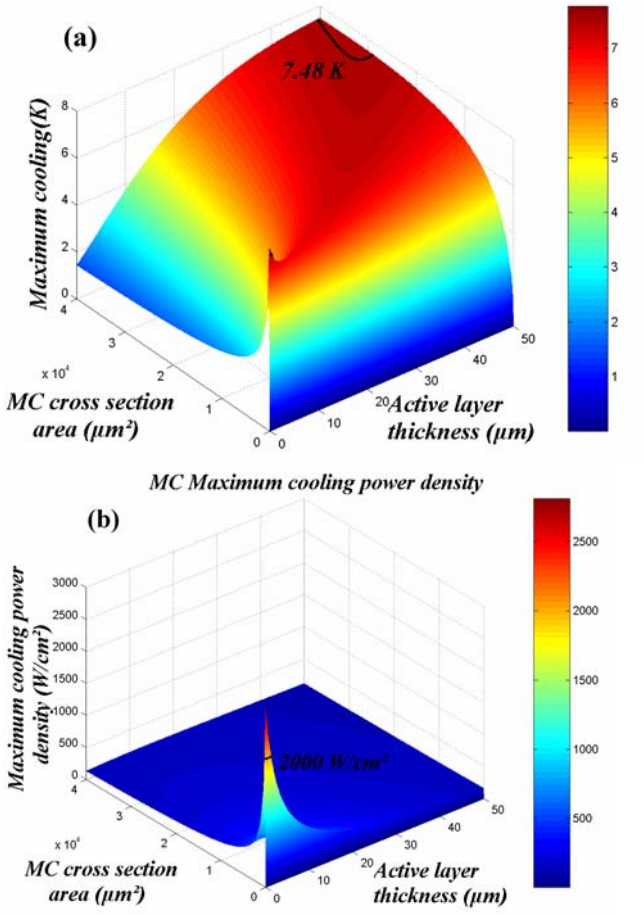

Figure 4: Calculated microrefrigerator maximum cooling (a) and maximum cooling power density (b) as a function of the microrefrigerator cross sectional area and the active SiGe layer thickness. In figure (a), the black contours show the maximum cooling value within the range of the used variables, and in figure (b), the black contour show a particular value of 2000 W/cm^2 just as a reference.

In figures 5 (a) and (b), we have plotted the variation of the maximum cooling and the maximum cooling power density at the microrefrigerator top surface, respectively, as a function of the microrefrigerator cross sectional area for different values of R_C^{Ohm} for the realistic case with the top side heat leakage within the metal lead considered. In both figures, there is an optimum size of the microrefrigerator. The results are very sensitive to R_C^{Ohm}; by increasing the contact resistance, the maximum cooling and the maximum cooling power density decreases and the optimum size increases.

The existence of an optimum device size can be understood as a consequence of the interplay between many competing effects. In fact the main factors limiting the maximum cooling are the total electrical and thermal parasitic resistances at the top side of the cooler and also the spreading

resistances in the substrate. Small size devices have large electrical and thermal resistances, but they have a small optimum current for maximum cooling and a low thermal leakage. On the other hand, for large devices, electrical and thermal resistances are small; the optimum current for maximum cooling is large, and the thermal leakage is more significant. Since the heating terms (due to Joule effect) depend quadratically on current, while the cooling terms (due to Peltier effect) depend linearly on current, a trade-off between these parameters gives an optimum device size.

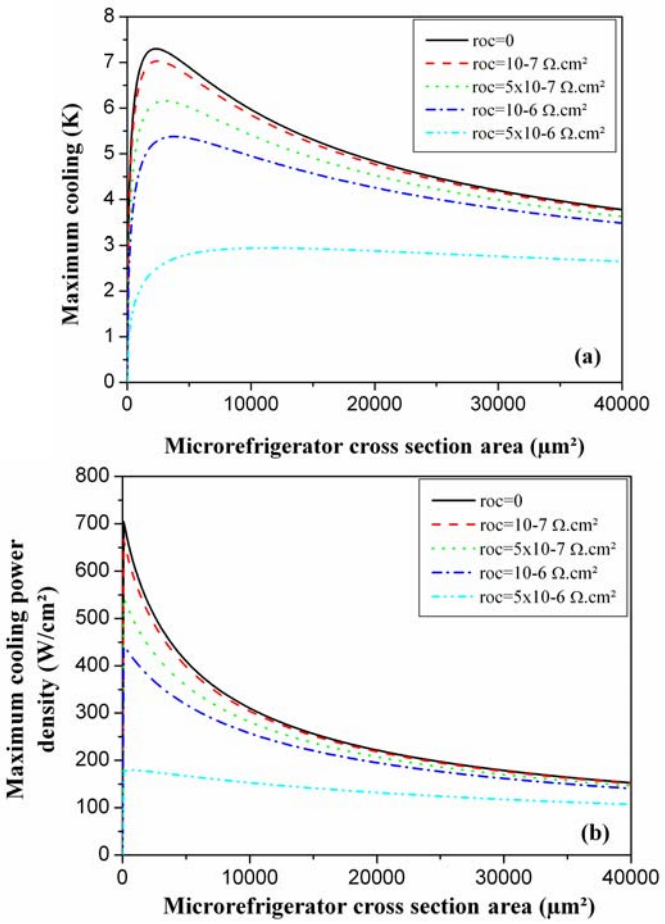

Figure 5: Calculated maximum cooling (a) and and the maximum cooling power density (b) as a function of the device cross section area for different Ohmic contact resistances values.

In order to optimize the cooling performance of the microrefrigerator device, we set the value of the Ohmic contact resistance at the metal/cap layers interface equal to a small realistic value which is about $10^{-7}\ \Omega.cm^2$. For this value, the optimum device size for the maximum cooling is about $50\times50\ \mu m^2$ as we can see in figure 5 (a). In the next discussions, we will keep this device size fixed as well as the value of R_C^{Ohm}.

Now that we have discussed, in some detail, how the geometrical parameters affect the cooling performance of microrefrigerators, let us take a look at the thermophysical properties. We will study the effect of the thermal and electrical conductivities of the active SiGe layer and the substrate. In figure 6, we have plotted the variation of the maximum cooling (a) and the maximum cooling power density (b) of a $50\times50\ \mu m^2$ microrefrigerator, as a function of the substrate thermal conductivity and the active SiGe layer thermal conductivity. By increasing the thermal conductivity of the active SiGe layer, both the maximum cooling and the maximum cooling power density decrease. On the other hand, by increasing the thermal conductivity of the substrate, the maximum cooling power density increases, whereas the maximum cooling decreases to rich a minimum and then starts to increase very slowly to saturate at about *1000 W/m/K*. After this value, the maximum cooling of the microrefrigerator becomes almost insensitive to the value of the substrate thermal conductivity. These results show the importance of using a high thermal conductivity substrate and a low thermal conductivity material as an active layer.

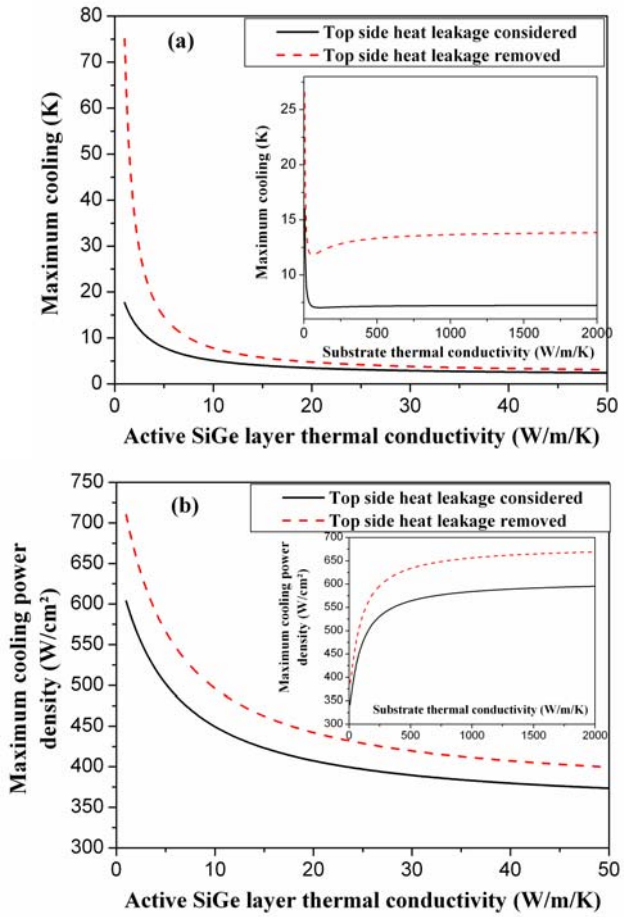

Figure 6: Calculated maximum cooling (a) and maximum cooling power density (b) of a $50\times50\ \mu m^2$ device with *10 μm* thick active SiGe layer as a function of the active SiGe layer thermal conductivity and the substrate thermal conductivity (the inset). In each case, the solid line corresponds to the current

realistic device with top side heat leakage, and the dashed line corresponds to the case without top side heat leakage.

In figures 7 (a) and (b), we show the effect of the electrical conductivity of the active SiGe layer and the substrate, respectively, on the maximum cooling of a $50x50\mu m^2$ device. The general trend is the same, by increasing the electrical conductivities, the maximum cooling of the microrefrigerator increase. The dependence on the thermal and electrical conductivities of the substrate and the active SiGe layer can easily be explained. Increasing thermal conductivities increases the heat conduction between the top and the bottom of the microrefrigerator, while increasing electrical conductivities decreases Joule heating. The latter enhances the cooling performance while the former degrades it.

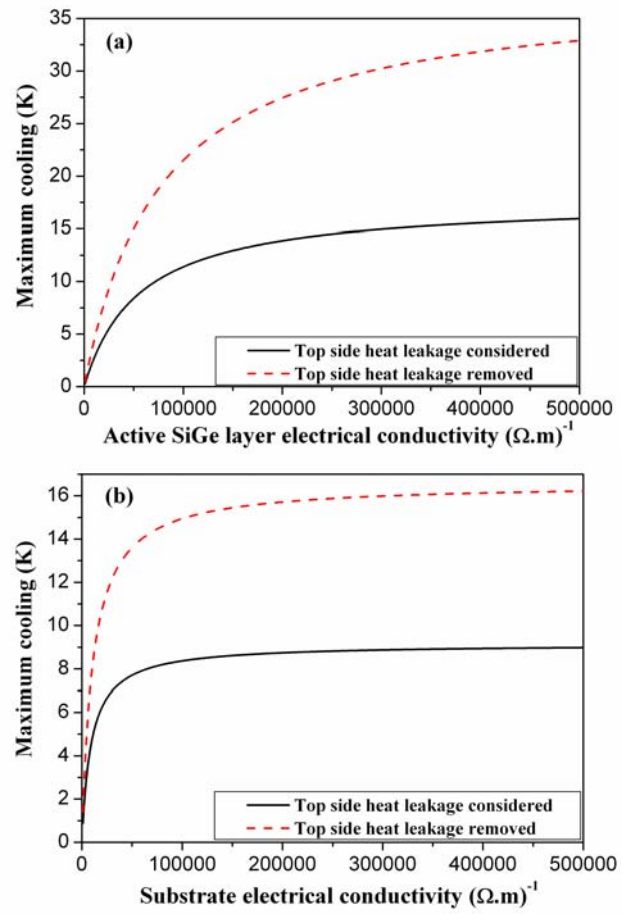

Figure 7: Calculated maximum cooling of a $50\times50\ \mu m^2$ device with $10\ \mu m$ thick SiGe layer as a function of the active SiGe layer electrical conductivity (a) and the substrate electrical conductivity (b). In each case, the solid line corresponds to the current realistic device with top side heat leakage, and the dashed line corresponds to the case without top side heat leakage.

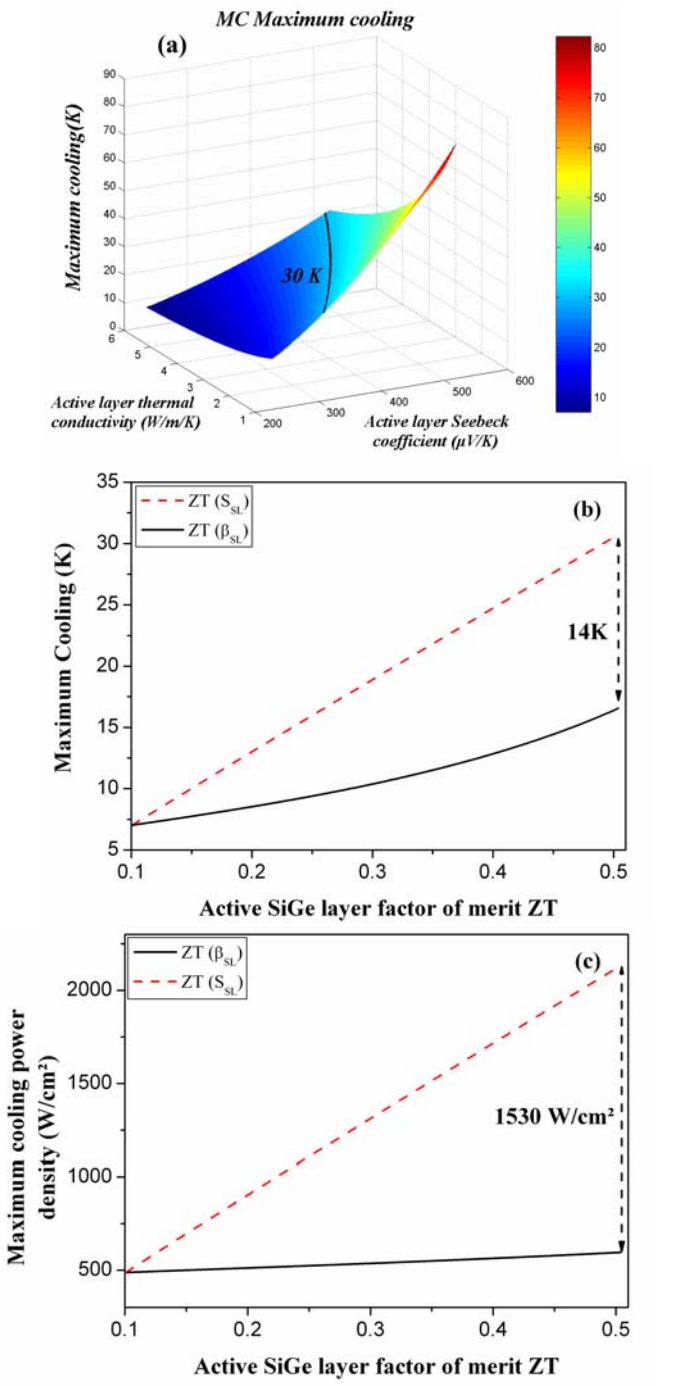

Figure 8: (a) Calculated maximum cooling as a function of the active SiGe layer thermal conductivity and Seebeck coefficient. The black contour show the value of 30 K. (b) and (c) correspond to the calculated maximum cooling and the maximum cooling power density, respectively, as a function of the active SiGe layer ZT. The solid line corresponds to ZT change due to the thermal conductivity variation, and the dashed line corresponds to ZT change due to the Seebeck coefficient variation, the electrical conductivity was kept constant.

Finally, let's study maximum cooling and maximum cooling power density as a function of the active layer factor of merit *ZT* including the effect of the thermal conductivity and the Seebeck coefficient. In figure 8 (a), we have plotted the calculated maximum cooling of the microrefrigerator as a function of the active layer thermal conductivity and Seebeck coefficient. The maximum cooling increases by increasing the Seebeck coefficient and/or decreasing the thermal conductivity as expected. The black line points the value of *30 K* (*10%* of room temperature). At cooling temperatures below *~30K*, our assumption on the temperature independence of the physical properties of the microrefrigerator are still valid as well as the fact that we can still keep the Peltier cooling power at interfaces independent of the cooling temperature (model linearity).

Figures 8 (b) and (c) show the calculated microrefrigerator maximum cooling and maximum cooling power density, respectively, as a function of the active layer *ZT*. We have plotted this dependence for two cases; the first case corresponds to the variation of *ZT* due to the variation of the thermal conductivity, and the second case corresponds to the variation of *ZT* due to the variation of the Seebeck coefficient. The electrical conductivity is assumed to be constant. To be able to compare the two parameters, the power factor σS^2 is increased by the same factor by which the thermal conductivity β is decreased. As we can see in figure 8, both the maximum cooling (b) and the maximum cooling power density (c) are more sensitive to the power factor variation than to the thermal conductivity variation. This behavior proves the advantage of using a superlattice structure as an active layer. As we have seen above, with these structures we can achieve higher power factors.

In figure 9, the cooling (a) and the maximum cooling power density (b) of the microrefrigerator are plotted as a function of the excitation current for two different values of the active SiGe layer figure of merit *ZT*.

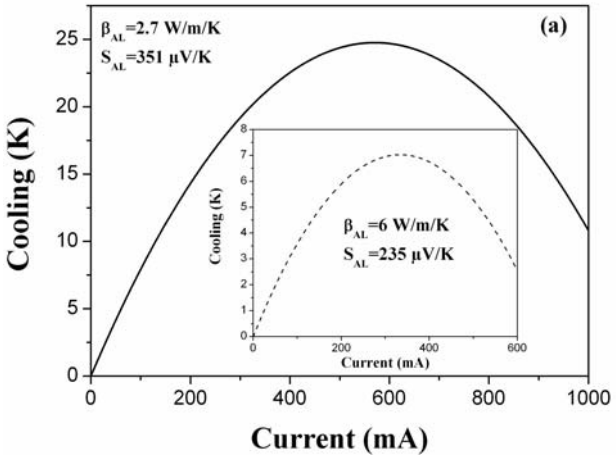

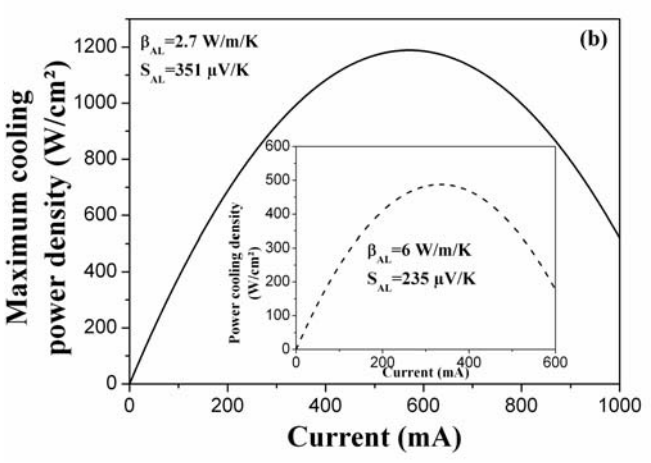

Figure 9: Calculated microrefrigerator cooling (a) and maximum cooling power density (b) as a function of the applied current when the active layer figure of merit *ZT* is increased by a factor of *5*. The insets show the performance curves for the current devices.

The insets, with the dashed line, correspond to the existing SiGe material with *ZT=0.1*, we have a maximum cooling of about *7 K* and a maximum cooling power density of *485 W/cm²*. Multiplying *ZT* by *5* allows a maximum cooling of about *24.75 K* and a maximum cooling power density of *1188 W/cm²*, which are more than *200%* higher for the cooling and more than *150%* higher for the maximum cooling power density, than the current values. We can see also that the optimum current is almost doubled.

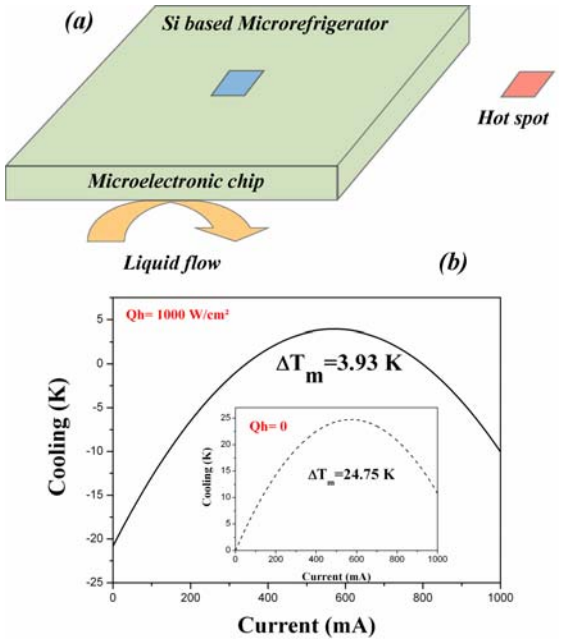

Figure 10: (a) Schema of the model configuration for combining microrefrigerator cooling with liquid cooling. (b) Variation of the microrefrigerator cooling as a function of the applied current for a heat load of *1000 W/ cm²*, in comparison with the case of zero heat load (the inset).

In figure 10, we give an example to demonstrate microrefrigerator's effectiveness to remove hot spots in an integrated circuit, and the further advantage we can get by combining this technique with liquid cooling technique. We assume a $50\times50\ \mu m^2$ hot spot with a heat load of $1000\ W/cm^2$ located at the center of a ($1cm\times1cm\times500\mu m$) microelectronic chip with an average heat load of $100\ W/cm^2$. In this simulation, we calculate the temperature profile on top of the chip with and without the microrefrigerator integrated underneath the hot spot. The heat sink is assumed to be operating at $70\ °C$ with a convection coefficient of $1.3\ W/cm^2/K$ [2]. Let's assume R_{Chip}^{Th}, A, and h are the thermal resistance of the chip, its cross sectional area, and the convection coefficient at its back side, respectively. $\overline{T_{ave}}$, and $\overline{\varphi_{ave}}$ are the average temperature and heat flux at the chip top side. T_∞, and φ_∞ are the room temperature and the heat flux at the chip back side (heat sink). We can write $\overline{T_{ave}}$ as a function of $\overline{\varphi_{ave}}$:

$$\overline{T_{ave}} - T_\infty = \left(R_{Chip}^{Th} + \frac{1}{hA} \right) \overline{\varphi_{ave}} \quad (12)$$

For a silicon chip with a thermal conductivity of $130\ W/m/K$, the chip heats up to $\overline{T_{ave}} - T_\infty \approx 81^\circ C$. Regarding the local character of the hot spot, the temperature at its top side is calculated assuming the chip as a semi-infinite medium, and then is expressed as [3]:

$$\overline{T_{HS}} - \overline{T_{ave}} = \pi r_0^2 \overline{\varphi_{HS}} R_{Chip}^{Sub} = \frac{8 r_0 \overline{\varphi_{HS}}}{3\pi \beta_{Chip}} \quad (13)$$

where $r_0 = \sqrt{A/\pi}$, β_{Chip} is the thermal conductivity of the silicon chip, and $\overline{\varphi_{HS}}$ is the heat load density at the top of the hot spot. Using this expression, we find that the hot spot heats up to $\overline{T_{HS}} - T\infty \approx 83^\circ C$, 2°C above the average temperature at the front side of the microelectronic chip. The microrefrigerator integrated underneath the hot spot is assumed to have a $10\ \mu m$ SiGe layer with a factor of merit $ZT=0.5$ with side metal contact geometry optimized as described earlier in the paper. When we integrate this microrefrigerator at the hot spot and apply an optimum current of $570\ mA$, the hot spot cools down to $\sim79°C$, which is $2°C$ below the chip average temperature. Figure 10 (b) recapitulates this behavior, where we can see that even with a heat load of $1000\ W/cm^2$, the microrefrigerator allows us to have a maximum cooling of $\sim4°C$, whereas for a zero heat load at the top microrefrigerator surface, the maximum cooling was $\sim25°C$. Improving the convection conditions by using for example direct liquid cooling at the back side of the chip makes the whole chip temperature drops down even more.

This simple example shows clearly the effectiveness of microrefrigerators in removing hot spots from the microelectronic chip. If we wanted to lower the maximum temperature of the chip (from $83°C$ to $81°C$) by only increasing the power of liquid cooling system, heat sink had to dissipate an additional $2.5W$, while the solution that includes monolithic microrefrigerator device require only a power of $\sim0.237W$.

CONCLUSION

The Thermal quadrupoles method is used to calculate the performance of Si/SiGe based microrefrigerators in the steady state regime. The maximum cooling and the maximum cooling power density of the device were studied as a function of different geometrical and material properties. We emphasized the effect of the substrate and the active SiGe layer properties. Simulation results match well the existing experimental data and they show the existence of an optimum device size and an optimum active layer thickness for maximum cooling performance. Existence of the optimum size is closely related to the top side heat leakage and the electrical spreading resistance in the substrate. Simulations also demonstrate the effect of the ohmic contact resistance at the metal /cap layer interface. This parameter is mainly dependant on the cleanliness of the sample surface and metallization and annealing conditions. Minimizing this parameter by increasing doping in the cap layer or decreasing the potential barrier between the metallic layer and the cap layer is very important.

The localized cooling performance of Si/SiGe based microrefrigerators makes them a potential candidate to be combined with liquid cooling techniques which offer an additional degree of freedom for thermal management in different length scales.

ACKNOWLEDGMENTS

The authors would like to thank IFC for supporting this work.

REFERENCES

[1]: D. M. Rowe, "Handbook of Thermoelectrics", CRC, 1995.

[2]: A. B. Cohen, M. Arik, and M. Ohadi, Proceeding of the IEEE, **94**, 1549-1570 (2006).

[3]: D. Maillet, S. André, J. C. Batsale, A. Degiovanni, and C. Moyne, THERMAL QUADRUPOLES: *Solving the Heat Equation through Integral Transforms* (John Wiley & Sons, 2000).

[4]: L. D. Patino-Lopez, S. Grauby, Y. Ezzahri, W. Cleays, and S. Dilhaire, Proceeding of the 25rd International Conference on Thermoelectrics, Vienna, Austria, August 6-10, (2006).

[5]: L. D. Patiño-Lopez, PhD Thesis, ON 2792, University Bordeaux 1, (2004).

[6]: Y. Ezzahri, S. Dilhaire, S. Grauby, L. D. Patiño-Lopez, W. Claeys, Y. Zhang, Z. Bian, and A. Shakouri, Proceeding of the 24rd International Conference on Thermoelectrics, pp. 241-245, Clemson, South Carolina, USA, June 19-23, (2005).

[7]: D. Vashaee, C. Labounty, X. Fan, G. Zeng, P. Abraham, J. E. Bowers, and A. Shakouri, Proceedings of the SPIE-The International Society for Optical Engineering, **4284**, 139-144, (2001).

[8]: D. Vashaee, J. Christofferson, Yan Zhang, A. Shakouri, G. Zeng, C. Labounty, X. Fan, J. E. Bowers, and E.

Croke, Microscale Thermophysical Engineering, **9**, 99-118, (2005).

[9]: Y. Zhang, G. Zeng, R. Singh, J. Christoffersen, E. Croke, J. E. Bowers and A. Shakouri, Proceeding of the 21st International Conference on Thermoelectrics, pp. 329-332, Long beach, California, USA, August 25–29, (2002).

[10]: Y. Ezzahri, PhD Thesis, ON 3090, University Bordeaux 1, (2005).

[11]: A. Shakouri and J. E. Bowers, Appl. Phys. Let, **71**, 1234, (1997).

[12]: A. Shakouri, E. Y. Lee, D. L. Smith, V. Narayanamurti, and J. E. Bowers, Micro. Therm. Eng, **2**, 37, (1998).

[13]: G. D. Mahan, and L. M. Woods, Phys. Rev. Let **80**, 4016, (1998).

[14]: A. Shakouri, Proceeding of the 24rd International Conference on Thermoelectrics, pp. 492-497, Clemson, South Carolina, USA, June 19-23, (2005).

[15]: J. M. Ziman, *Electrons and Phonons*, C. Press, Oxford, (1960).

[16]: S. Dilhaire, Y. Ezzahri, S. Grauby, W. Claeys, J. Christofferson, Y. Zhang, and A. Shakouri, Proceeding of the 23rd International Conference on Thermoelectrics, pp. 519-523, La Grande Motte, France, August 17-21, (2003).

[17]: P. Wang, A. B. Cohen, B. Yang, G. L. Solbrekken, and A. Shakouri, J. Appl. Phys, **100**, 014501, (2006).

[18]: K. J. Negus, M. M. Yovanovich, and D. J. Roulston, Proceeding of the ASME/JSME Thermal Engineering Joint Conference, pp. 395-401, (1987).

[19]: Y. Ezzahri, R. Singh, J. Christofferson, Z. Bian, and A. Shakouri, (upcoming paper).

[20]: Y. Zhang, D. Vashaee, J. Christofferson, G. Zeng, C. LaBounty, J. Piprek, E. T. Croke, and A. Shakouri, Proceeding of the International Mechanical Engineering Congress and Exposition, Washington DC, USA, November 16-21, (2003).

[21]: S. T. Huxtable, A. R. Abramson, C. L. Tien, A. Majumdar, C. LaBounty, X. Fan, G. Zeng, J. E. Bowers, A. Shakouri, and E. T. Croke, Appl Phys Let, **80**, 1737, (2002).

[22]: Y. Ezzahri, G. Zeng, K. Fukutani, Z. Bian, and A. Shakouri, Proceeding of the Thermal Challenges in Next Generation Electronic Systems II conference, pp. 111-118, Santa Fe, USA, January 7-10, (2007).